

# Optical Engineering

OpticalEngineering.SPIEDigitalLibrary.org

## Topological properties of optical fields: description of morphogenesis and bifurcations in focusing regions

Saul I. De Los Santos Garcia  
Marco A. Torres Rodriguez  
Mayra Vargas Morales  
Patricia Martinez Vara  
Andrea Garcia Guzman  
Gabriel Martinez Niconoff

**SPIE.**

Saul I. De Los Santos Garcia, Marco A. Torres Rodriguez, Mayra Vargas Morales, Patricia Martinez Vara, Andrea Garcia Guzman, Gabriel Martinez Niconoff, "Topological properties of optical fields: description of morphogenesis and bifurcations in focusing regions," *Opt. Eng.* **56**(11), 115102 (2017), doi: 10.1117/1.OE.56.11.115102.

# Topological properties of optical fields: description of morphogenesis and bifurcations in focusing regions

Saul I. De Los Santos Garcia,<sup>a</sup> Marco A. Torres Rodriguez,<sup>a</sup> Mayra Vargas Morales,<sup>a</sup> Patricia Martinez Vara,<sup>b</sup> Andrea Garcia Guzman,<sup>a</sup> and Gabriel Martinez Niconoff<sup>a,\*</sup>

<sup>a</sup>Instituto Nacional de Astrofísica, Óptica y Electrónica INAOE, Departamento de Óptica, Puebla, Mexico

<sup>b</sup>Benemerita Universidad Autónoma de Puebla, BUAP Av. San Claudio s/n, Puebla, Mexico

**Abstract.** We analyze the diffraction field when changes in the curvature function of the boundary condition are implemented. The study is performed using differential geometry models with a curvature function displaying local behavior. Depending on the sign of curvature, we classify the diffraction field as elliptic, hyperbolic, or parabolic. In particular, it is shown that the optical field is organized around the parabolic regions, which correspond to focusing regions. The model is experimentally corroborated by applying a coordinate transformation to the transmittance of a zone plate. The reason to use this transmittance comes from the fact that its diffraction field displays multiple foci allowing identification, description, and control of bifurcations and morphogenesis effects, which are studied using the curvature function. © The Authors. Published by SPIE under a Creative Commons Attribution 3.0 Unported License. Distribution or reproduction of this work in whole or in part requires full attribution of the original publication, including its DOI. [DOI: [10.1117/1.OE.56.11.115102](https://doi.org/10.1117/1.OE.56.11.115102)]

Keywords: morphogenesis; bifurcation; focusing regions.

Paper 170826P received May 31, 2017; accepted for publication Oct. 23, 2017; published online Nov. 10, 2017.

## 1 Introduction

The physical features of optical fields can be obtained from the phase function, and this is implicit in the solution of the Helmholtz equation, when an equation relating the amplitude and phase is deduced. When the phase is compressed to a minimum volume, the amplitude reaches its maximum value, corresponding to a focusing region. In these regions, the wavefront curvature is reversed and new physical properties can emerge. For example, the optical field can be split into two or more branches, known as a bifurcation effect, as a consequence of the continuous evolution of a parameter (which can be the propagation distance). Closely related to this effect is the change in the geometry of the optical field, which is the morphogenesis effect. This effect originates in the neighborhood of focusing regions that correspond to the organization regions for the entire optical field.<sup>1-3</sup> In a diffraction field, the focusing regions, also known as caustic regions, correspond to Fraunhofer diffraction, as will be shown below. The topological properties of these areas offer interesting applications, such as the design of dynamical optical tweezers for particle trapping and hybrid lens design. From a theoretical point of view, interesting properties, such as the induction of tunable spectroscopy as well as the generation of vortices and topological charges, can be studied.<sup>4-12</sup>

In this paper, we present a study of the spatial evolution of optical fields generated by diffraction when a coordinate transformation is implemented in the transmittance function. This transformation generates nonlinear changes in the curvature function  $k_0$  whose expression for a curve  $y = f(x)$  is

$$k_0 = \frac{f''(x)}{\{1 + [f'(x)]^2\}^{\frac{3}{2}}}. \quad (1)$$

The nonlinear effects are manifested as abrupt changes in the envelope curve geometry generated by the curvature centers, known as evolutes.<sup>13</sup> In an optical context, this corresponds with the focusing region. It is known that the manifestation of the nonlinearities has associated shock waves,<sup>14,15</sup> justifying that the optical field presents physical effects with interesting topological properties in the neighborhood of focusing regions. Our analysis was performed using results from differential geometry, particularly Euler's theorem.<sup>16</sup> The theoretical model was experimentally corroborated using, as a prototype, a boundary condition type zone plate (ZP). This transmittance was chosen because it makes it easy to detect the presence of morphogenesis and bifurcation at every focus. These effects consist of unfolding the focus into two or more focusing regions with different geometries. Furthermore, Euler's theorem allows the classification of the nature of the optical fields as parabolic, hyperbolic, or elliptic. It is shown below that the focusing regions correspond to parabolic zones that act as organization regions for the entire optical field, separating the hyperbolic and elliptic regions. Evolution of the hyperbolic regions is explained by describing the angular changes among the asymptotes. This analysis is important, because the conditions under which the optical field can transfer angular momentum are obtained. Experimental results for the transformed ZPs lead us to identify that each focus evolves following hyperbolic or elliptical regions, depending on its order. A relevant finding of the study is that the parabolic region is matched with the Fraunhofer diffraction and that from this perspective, the calculus of the diffraction integral can be avoided.

\*Address all correspondence to: Gabriel Martinez Niconoff, E-mail: [gmartin@inaoep.mx](mailto:gmartin@inaoep.mx)

## 2 Theory

We start the study describing some concepts of differential geometry. The surface under study has a biparametric representation, given by

$$\vec{X}(u, v) = [x(u, v), y(u, v), z(u, v)], \quad (2)$$

where  $u$  and  $v$  are the parameters known as curvilinear coordinates. The case  $u = \text{constant}$  defines a curve placed on the surface, as does for  $v = \text{constant}$ . The partial derivatives denoted by  $\vec{X}_u$  and  $\vec{X}_v$  are the two vectors tangent to the respective curves. From this result, we obtain that the surface has an associated unitary normal vector  $\hat{N}$ , given by

$$\hat{N} = \frac{\vec{X}_u \times \vec{X}_v}{|\vec{X}_u \times \vec{X}_v|}. \quad (3)$$

Consider an arbitrary curve on the surface, whose parametric description is given by

$$\vec{X}(s) = [x(s), y(s), z(s)], \quad (4)$$

where  $s$  is the arc-length. The unitary tangent vector  $\hat{T}(s)$  to the curve [Eq. (4)] is

$$\frac{d}{ds} \vec{X}(s) = \hat{T}(s). \quad (5)$$

Other geometrical properties of the curve can be obtained from the second derivative

$$\frac{d^2}{ds^2} \vec{X}(s) = k(s) \hat{n}(s) = \vec{K}(s), \quad (6)$$

where  $k(s)$  is the curvature function and  $\hat{n}(s)$  is a unit normal vector whose direction depends of the selected curve  $\vec{X}(s)$ ; however, generic features can be obtained from its decomposition. Representing the curvature vector  $\vec{K}(s)$  as

$$\vec{K}(s) = \vec{k}_N(s) + \vec{k}_g(s), \quad (7)$$

where  $\vec{k}_N(s)$  is known as the normal vector curvature parallel to  $\hat{N}$  and  $\vec{k}_g(s)$  is the geodesic curvature placed on the tangent plane. This set of vectors is sketched in Fig. 1.

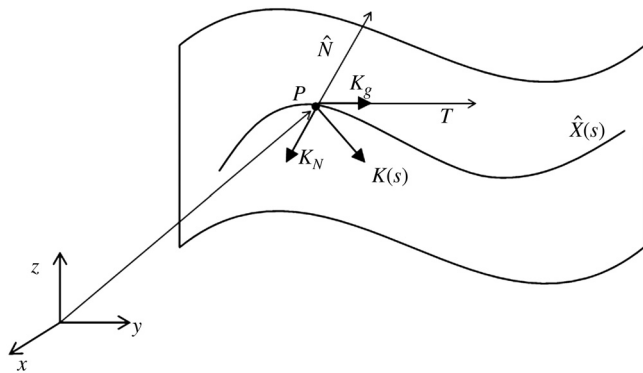


**Fig. 1** Vector description of an arbitrary curve  $\vec{X}(s)$  on the surface under study.

The modulus of the normal curvature vector carries the information about the surface geometry, and it is given by

$$k_N = \frac{\vec{X}_u \cdot \hat{N}_u du^2 + \vec{X}_v \cdot \hat{N}_v dv^2 + (\vec{X}_u \cdot \hat{N}_v + \vec{X}_v \cdot \hat{N}_u) du dv}{\vec{X}_u \cdot \vec{X}_u du^2 + \vec{X}_v \cdot \vec{X}_v dv^2 + 2\vec{X}_u \cdot \vec{X}_v du dv} = \frac{e du^2 + g dv^2 + 2f du dv}{E du^2 + G dv^2 + 2F du dv}, \quad (8)$$

where we have defined the terms as

$$\begin{aligned} e &= -\vec{X}_u \cdot \hat{N}_u; & g &= -\vec{X}_v \cdot \hat{N}_v; \\ 2f &= -\vec{X}_u \cdot \hat{N}_v + \vec{X}_v \cdot \hat{N}_u E = \vec{X}_u \cdot \vec{X}_v; \\ G &= \vec{X}_v \cdot \vec{X}_v; & F &= \vec{X}_u \cdot \vec{X}_v. \end{aligned} \quad (9)$$

Equation (8) corresponds to the quotient of the fundamental forms of differential geometry, more details can be found in Ref. 16. One important behavior of the surface is obtained when  $k_N = 0$ , implying the vector curvature  $\vec{K}(s)$  is placed on the tangential plane; this occurs when

$$e du^2 + g dv^2 + 2f du dv = 0. \quad (10)$$

The last equation can be rewritten as

$$g \left( \frac{dv}{du} \right)^2 + 2f \left( \frac{dv}{du} \right) + e = 0, \quad (11)$$

which corresponds to a quadratic form for the derivative  $\frac{dv}{du}$ , satisfying

$$\frac{dv}{du} = \frac{-f \pm \sqrt{f^2 - ge}}{g}. \quad (12)$$

The nature of the derivative  $\frac{dv}{du}$  depends on the sign of the discriminant  $f^2 - ge$  and has the following classifications:

- (i)  $f^2 - ge = 0 \rightarrow$  parabolic region
- (ii)  $f^2 - ge > 0 \rightarrow$  hyperbolic region
- (iii)  $f^2 - ge < 0 \rightarrow$  elliptic region. (13)

This last statement constitutes the Euler's theorem for surface classification, more details can be found in Ref. 16.

The previous analysis is now transferred to an optical context, where the diffraction field has an associated biparametric phase function. We will show that the focusing regions correspond to parabolic regions; these regions in the diffraction field are also matched with the Fraunhofer diffraction. The Fresnel diffraction evolves following hyperbolic or elliptic regions; for the hyperbolic case, two asymptotes can be identified, and the elliptic regions do not present asymptotes. The parabolic regions occur when the curvature of Eq. (12) takes a single value given by

$$\frac{dv}{du} = -\frac{f}{g}. \quad (14)$$

The geometrical interpretation is the tangent vectors  $\vec{X}_u$  and  $\vec{X}_v$  become parallel. The parabolic regions have an associated nonlinear partial differential equation for the phase function  $L = L(u, v)$  given by

$$f^2 - ge = \left( \frac{\partial^2 L}{\partial u \partial v} \right)^2 - \frac{\partial^2 L}{\partial u^2} \frac{\partial^2 L}{\partial v^2} = 0, \quad (15)$$

where  $u$  and  $v$  are the two parameters that can be the spatial frequencies.

It should be noted that the previous equation is the null value of the Hessian determinant in catastrophe theory, thus parabolic regions correspond with the singularities of optical fields<sup>17</sup> also known as caustic or focusing regions. By implementing Eq. (15) in the diffraction integral, it is easy to show that the quadratic factors cancel, corresponding to Fraunhofer diffraction and meaning that parabolic regions are the organization regions of the optical field. It must be noted that in Fresnel diffraction the Hessian determinant is nonzero and that catastrophe theory is, therefore, not applicable. Analyzing the quadratic form of Eq. (11), we have that the hyperbolic region is bounded by its asymptotes, which separates regions of curvature with different signs. The elliptic case does not have asymptotic directions because  $\frac{du}{dv}$  has complex values, and the normal curvature does not reverse the sign. Consequently, the surface of this region is always either convex or concave. The previous analysis will be experimentally implemented on a transformed ZP in Sec. 3.

### 3 Description of Focusing Regions: Topological Properties of Optical Fields

The previous analysis can be better understood when it is applied to describe an optical field. A great variety of optical elements generate optical foci when they are illuminated, classical examples being lenses and ZPs. In this paper, we consider only ZP. In an ideal aberration free system, the focusing geometry corresponds to a set of points distributed along a line perpendicular to the ZP plane. The transmittance function for a ZP<sup>18</sup> is

$$t(x, y) = \sum_{n=-\infty}^{\infty} a_n e^{i2\pi(x^2+y^2)\frac{n}{d^2}}. \quad (16)$$

It is easy to show that this last expression can be obtained as a quadratic transformation for the Fourier series of a linear grating. When the ZP is illuminated with a plane wave, the foci coordinates are given by  $x = y = 0$ ,  $z = \frac{d^2}{2n\lambda}$ , where  $\lambda$  is the wavelength of the light. We remark that the foci position depends on the diffraction order defined by integer  $n$ , and that the diffraction field can be considered as a set of surfaces where each one generates a single focus. With the purpose to analyze the topological properties of the foci, we propose a coordinate transform given by  $x \rightarrow ax$ ,  $y \rightarrow by$ , the transmittance function for the transformed ZP acquires the form

$$t(x, y) = \sum_{n=-\infty}^{\infty} a_n e^{i2\pi(a^2x^2+b^2y^2)\frac{n}{d^2}}. \quad (17)$$

Without loss of generality, we can assume that  $a > b$  with  $a, b \in \mathbb{R}$ . The diffraction field is given by

$$\begin{aligned} \phi(x_0, y_0, z, n) \\ = \sum_{n=-\infty}^{\infty} a_n \iint e^{i2\pi(a^2x^2+b^2y^2)\frac{n}{d^2}} e^{i\frac{\pi}{\lambda z}(x^2+y^2)} e^{-i2\pi\left(\frac{x_0^2}{\lambda z} + \frac{y_0^2}{\lambda z}\right)} dx dy, \end{aligned} \quad (18)$$

identifying the phase function as

$$\begin{aligned} L(x_0, y_0, z) = & \left(2\frac{a^2n}{d^2} + \frac{1}{\lambda z}\right)x^2 + \left(2\frac{b^2n}{d^2} + \frac{1}{\lambda z}\right)y^2 \\ & - x\frac{x_0}{\lambda z} - y\frac{y_0}{\lambda z}, \end{aligned} \quad (19)$$

where some common terms have been omitted. The phase function is interpreted as a set of trajectories whose envelope generates the focusing region. It has a biparametric representation where the  $x$  and  $y$  parameters are placed on the boundary condition; for this reason, we can apply differential geometry results described in Sec. 2. Substituting Eq. (19) in Eq. (15) is easy to show that quadratic terms are cancelled corresponding to the Fraunhofer diffraction. The nature of the optical field can be obtained with Eq. (13) and its geometry type is obtained with the sign of the determinant to the quadratic form, i.e.,

$$\Delta(z, a, b) = \begin{pmatrix} 2\frac{a^2n}{d^2} + \frac{1}{\lambda z} \\ 2\frac{b^2n}{d^2} + \frac{1}{\lambda z} \end{pmatrix} \begin{pmatrix} > 0 \\ = 0 \\ < 0 \end{pmatrix}. \quad (20)$$

The curve is an ellipse when  $\Delta(z, a, b) > 0$ , and when  $\Delta(z, a, b) < 0$ , it corresponds to a hyperbolic curves. The geometry of the focusing region is obtained when  $\Delta(z, a, b) = 0$ , and it must be analyzed by considering other properties of the optical surface, as shown below. From Eq. (19), we identify the distance along the  $z$ -coordinate where focusing is generated. It occurs at two  $z$ -coordinate positions given by

$$2\frac{a^2n}{d^2} + \frac{1}{\lambda z} = 0, 2\frac{b^2n}{d^2} + \frac{1}{\lambda z} = 0. \quad (21)$$

Analyzing the first term, we have that the focusing occurs at

$$z(n, a) = -\frac{d^2}{2a^2n\lambda}. \quad (22)$$

To achieve a real focusing, i.e.,  $n < 0$ , the positive values correspond to virtual focusing. Using this result, in the diffraction integral given by Eq. (18), it is easy to show that the focusing region has a linear shape along the  $y$ -coordinate, and a similar behavior can be shown for the second term in Eq. (21) in that the focusing region has a linear shape along the  $x$ -coordinate. Next, we analyze how the optical surface evolves between focusing regions. For this, we consider a small change in the  $z$ -coordinate given by  $z(n, a) \pm \epsilon$

$$z(n, a) - z' = -\frac{d^2}{2a^2n\lambda} - z' = \epsilon. \quad (23)$$

When  $\epsilon > 0$ ,  $z'$  is less than  $z(n, a)$ , corresponding to elliptical surfaces. Analyzing the inequality given by Eq. (20), it is easy to deduce that both hyperbolic and elliptical regions may coexist in the same diffraction field for different diffraction  $n$ -orders, consequently the evolution of each foci presents different topological properties. Analyzing first the hyperbolic region and considering  $\epsilon < 0$ , the optical

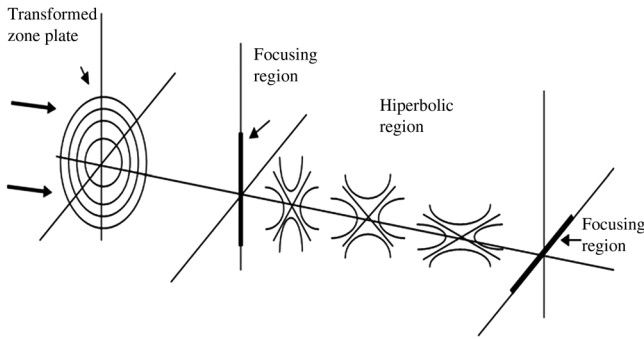


**Fig. 2** Graphical description of the bifurcation effects. The focus is split into two focusing regions following a parabolic–hyperbolic–parabolic sequence.

surface geometry is a set of hyperbolae whose asymptotes are

$$y = \pm \frac{\sqrt{2 \frac{a^2 n}{d^2} + \frac{1}{\lambda z}}}{\sqrt{2 \frac{b^2 n}{d^2} + \frac{1}{\lambda z}}} x, \quad (24)$$

where  $z$  satisfies  $z(n, a) < z < z(n, b)$ . It is easy to deduce that the focusing region is generated when the asymptotes becomes parallel, as sketched in Fig. 2. This behavior lets us explain the transition from hyperbolic to parabolic regions on a geometrical basis, allowing us to understand the physical properties of astigmatic optical systems.

The experimental setup consisted of a transformed ZP illuminated with a plane wave. The transformed resulting ZP with parameters  $a = 1$ ,  $b = 0.8$  and the resulting evolution of the diffraction field associated with the first focus is shown in Fig. 3.

In circular ZPs, the geometry of the focusing regions is points distributed along the  $z$ -axis. In the transformed ZP,

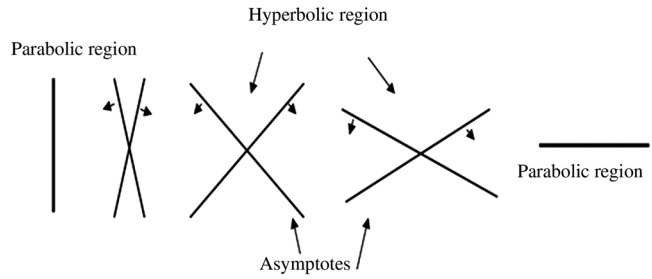


**Fig. 4** The hyperbolic behavior bounded by the angular changes among the asymptotes. This justifies the morphological changes of the optical field.

each focal point is split into two focusing line regions, which is a classic effect of astigmatic systems; this is interpreted as bifurcation and morphogenesis effects at each focus. We note that the synthesis of focusing regions occurs when the asymptotes of the hyperbolic region becomes parallel, having two possibilities as shown in Fig. 4.

From this geometrical interpretation, we can predict the angular momentum transfer, which implies a nonsymmetrical evolution of the asymptotes. This can be done by propagating the optical field in a medium with a variable refractive index, leading to the generation of optical vortices. Other important behavior, for the same scaled ZP, can be deduced from Eq. (23). This is obtained considering the integer  $n$  large enough such that parabolic–elliptical transitions are generated as it is shown in Fig. 5.

Other interesting results can be observed when the transformation is of the form  $x \rightarrow ax$ ,  $y \rightarrow iay$ , which generates a ZP with hyperbolic geometry as shown in Fig. 6. This transmittance maintains focusing capability with a similar geometry to the scaled ZP, as can be observed from the experimental results.

The analysis of the diffraction field is analogous to a scaled ZP. It is easy to show that two focusing regions

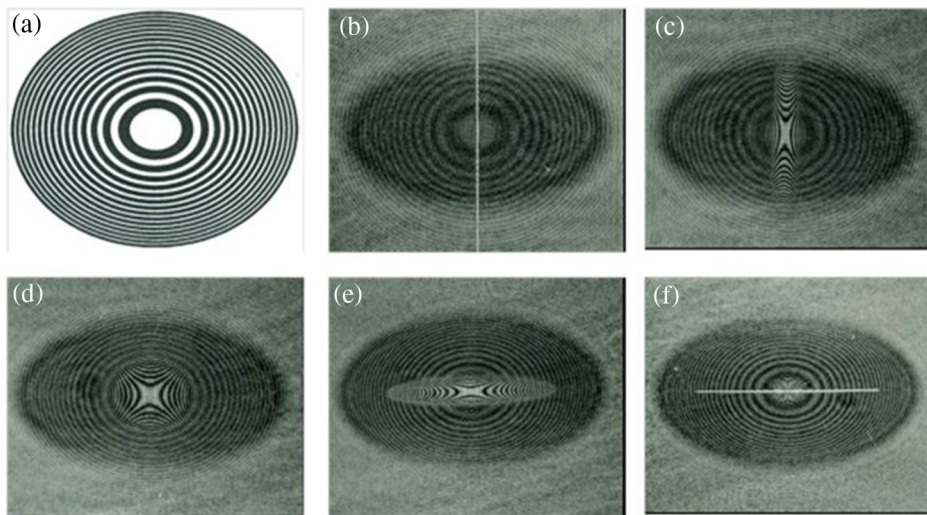


**Fig. 3** Irradiance distribution for the diffraction field (a) transformed ZP type elliptic. (b) and (f) Show the irradiance distribution for the focusing regions corresponding to a parabolic region. (c)–(e) Show regions of hyperbolic behavior. The diffraction field was generated illuminating the ZP with a plane wave emerging from a He–Ne laser of 632.8 nm. The ZP transmittance was recorded in a high-resolution plate with square geometry of 0.5 cm per side.

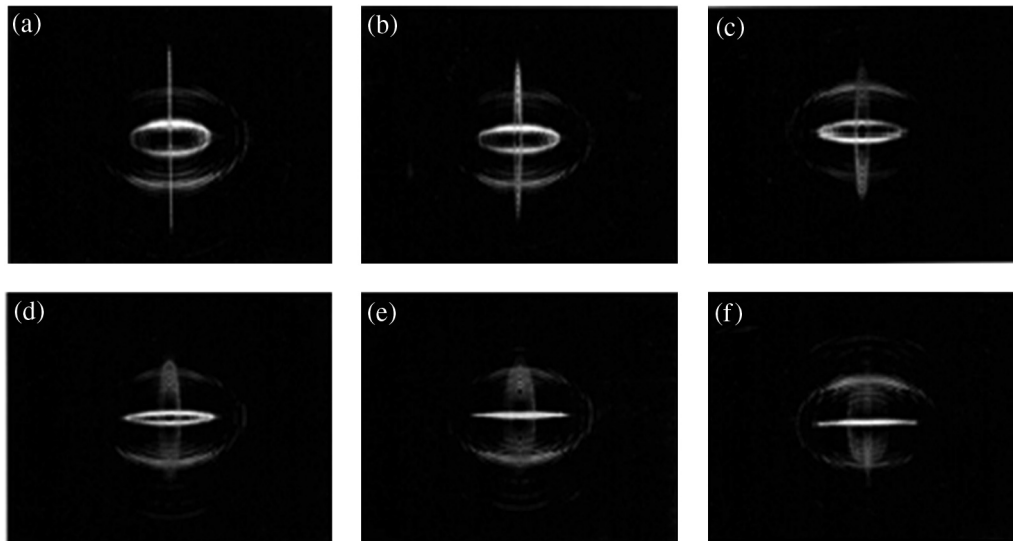


**Fig. 5** Irradiance distribution for the diffraction field for the transformed ZP of elliptic geometry. (a) and (f) Show the same geometry as shown in Fig. 3 and (b)–(e) regions of elliptic behavior.

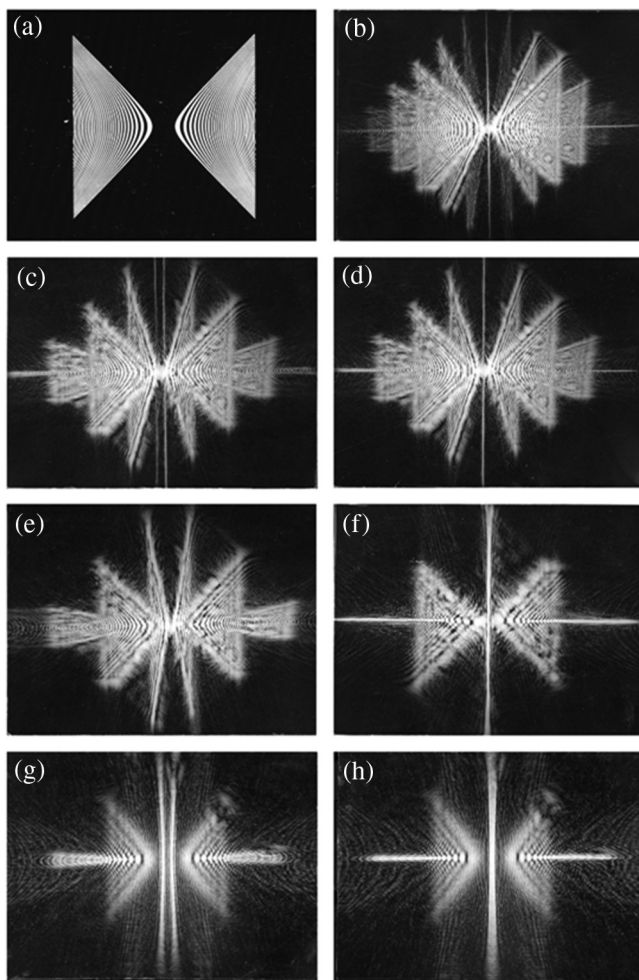


**Fig. 6** (a) Hyperbolic ZP and (b)–(f) evolution of the diffraction field between two focusing regions. The illuminating parameters and the size of the ZP are the same as described in Fig. 3.

corresponding to the diffraction order  $n$  and  $-n$  occurs on the same plane and that both regions are mutually perpendicular.

#### 4 Conclusions

We analyzed optical surfaces by means of differential geometry, using Euler's theorem to describe the spatial evolution of the curvature function. This analysis led to the classification of optical surfaces as elliptic, hyperbolic, and parabolic. This last region is very important, because it corresponds to the Fraunhofer diffraction, as can be deduced from the phase function in the diffraction integral. To obtain experimental results, we employed two transformed ZPs, showing that a simple transformation of the boundary condition is capable of generating two interesting effects. One of these effects is the morphogenesis process, the other is the generation of bifurcation effects in the Fraunhofer region, characterized by splitting the spatial distribution of the focusing regions, i.e., it consists of unfolding each focal point into multiple focusing regions. The transition between parabolic–hyperbolic regions was analyzed through the angular changes of its asymptotes. The parabolic regions occur when the asymptotes become parallel. The behavior of the asymptotes' evolution allows the calculation of the angular momentum and the generation of optical vortices. These properties can be implemented by breaking the symmetry in the angular changes of the asymptotes through making the optical field propagate in a medium with a variable refractive index.

The main results of the paper can be summarized as follows:

Optical fields were analyzed by implementing differential geometry models, allowing us to classify the optical regions as hyperbolic, elliptic, or parabolic.

The parabolic region corresponds to the Fraunhofer diffraction and can be identified applying the condition

$$\left(\frac{\partial^2 L}{\partial u \partial v}\right)^2 - \frac{\partial^2 L}{\partial u^2} \frac{\partial^2 L}{\partial v^2} = 0,$$

where  $L$  is the phase function. This condition is a consequence of the Euler's theorem. This approach avoids the calculus of the diffraction integral for the Fraunhofer region.

The transformation for each coordinate generates bifurcation effects in the focusing regions, allowing the incorporation of tunable/selective spatial filtering.

Morphogenesis processes are generated between two Fraunhofer regions. When the optical field displays a hyperbolic behavior, it has two associated asymptotes that allow the study of angular momentum transfer. The Fraunhofer regions correspond to the focusing regions, which occur when the asymptotes become parallel.

The topological structure for each focus presents elliptical or hyperbolic behavior, which implies that spatial filtering process depends on the focus order determined by the value of the integer  $n$ .

Finally, the model presented can be extended to implement other type of transformations of the form  $x \rightarrow ax + iby$ ,  $y \rightarrow cx + idy$ , generating ZPs with different geometries and offering applications to hybrid lenses design and the implementation of tunable spatial filtering process. Furthermore, the presented model has applications in the implementation of optical tweezers, the analysis of which will be presented in a forthcoming paper.

### Acknowledgments

The authors S.I.D.L.S.G., M.A.T.R., A.G.G., and M.V.M. are thankful to CONACyT for their support.

### References

1. M. V. Berry and C. Upstill, "Catastrophe optics: morphologies of caustics and their diffraction patterns," *Prog. Opt.* **18**, 257–323 (1980).
2. P. Martinez-Vara et al., "Diffraction by three-dimensional slit-shape curves: decomposition in terms of Airy and Pearcey functions," *Opt. Lett.* **40**(15), 3496–3499 (2015).
3. Y. S. Kivshar and E. A. Ostrovskaya, "Optical vortices folding and twisting waves of light," *Opt. Photonics News* **12**(4), 24–28 (2001).
4. C. K. R. T. Jones, T. Kupper, and K. Schaffner, "Bifurcation of asymmetric solution in nonlinear optical media," *Math. Phys.* **52**, 859–880 (2001).
5. J. Masajada and B. Dubik, "Optical vortex generation by three plane wave interference," *Opt. Commun.* **198**, 21–27 (2001).
6. M. Nikkhou et al., "Light-controlled topological charge in a nematic liquid crystal," *Nat. Phys.* **11**, 183–187 (2015).
7. P. Vaity and R. P. Singh, "Topological charge dependent propagation of optical vortices under quadratic phase transformation," *Opt. Lett.* **37**(8), 1301–1303 (2012).
8. M. V. Berry, "The adiabatic phase and Pancharatnam's phase for polarized light," *J. Mod. Opt.* **34**(11), 1401–1407 (1987).
9. S. Feng and H. G. Winful, "Physical origin of the Gouy phase shift," *Opt. Lett.* **26**(8), 485–487 (2001).
10. V. Y. Osipov, "Diffraction catastrophe in the focusing region of an aberrated laser beam and associated optical vortices," *J. Opt. Tech.* **66**(12), 1035–1037 (1999).
11. M. J. Padgett, J. Molloy, and D. McGloin, *Optical Tweezers: Methods and Applications*, CRC Press, Boca Raton, Florida (2010).
12. P. Prasad, *Nonlinear Hyperbolic Waves in Multidimensions*, CRC Press, Hoboken, New Jersey (2001).
13. N. Piskunov, *Calculo Diferencial e Integral*, Montaner y Simón, Barcelona (1983).
14. A. Gaponov Grekhov and M. I. Rabinovich, *Nonlinearities in Action: Oscillations Chaos Order Fractals*, Springer-Verlag, Berlin (1992).
15. R. Courant and K. O. Friedrichs, *Supersonic Flow and Shock Waves*, Springer, Berlin (1976).
16. J. Struik, *Lectures on Classical Differential Geometry*, Dover Publications, New York (1961).
17. V. I. Arnold, *Mathematical Methods of Classical Mechanics*, Springer, New York (1989).
18. J. Ojeda-Castañeda, A. Saucedo-Carvajal, and J. E. A. Landgrave, "Pseudo zone plate for extended focal depth," *Opt. Mem. Neural Networks* **18**(3), 164–170 (2009).

**Saul I. De Los Santos Garcia** received his PhD from Instituto Nacional de Astrofísica Óptica y Electrónica (INAOE) in 2016. His research is in the study of topological properties of optical fields, plasmon optics, and study of electromagnetic properties in rough surfaces.

**Marco A. Torres Rodriguez** received his MS degree from INAOE in 2014. His research involves analysis of surface plasmons singularities and diffraction optics theory.

**Mayra Vargas Morales** received her MS degree from INAOE in 2015. Her research involves optical solitons, liquid crystals, surface plasmons, and resonant effects in particle plasmons.

**Patricia Martinez Vara** received her PhD from INAOE in 2003. Her research is in the study of optical trapping of particles using focusing regions.

**Andrea Garcia Guzman** is an engineering physicist graduated from Iberoamerican University in 2016. Her lines of investigation are statistical optics, diffusion processes, and diffractive optics.

**Gabriel Martinez Niconoff** received his PhD from INAOE in 1995. His topics of research are related to analysis of dynamical systems and mathematical optics.